

ENHANCED HEAT CONDUCTION IN PHASE-CHANGE THERMAL ENERGY STORAGE DEVICES

RICHARD H. HENZE

and

JOSEPH A. C. HUMPHREY

Department of Mechanical Engineering, University of California,
 Berkeley, CA 94720, U.S.A.

(Received 21 April 1980 and in revised form 24 July 1980)

Abstract—Phase-change energy storage devices have an inherent disadvantage due to the insulating properties of the phase-change materials (PCM's) used. Such systems are difficult to analyze theoretically due to the nonlinearities of the moving liquid–solid interface and the presence of natural convection as shown by several recent numerical and experimental investigations. Previous work has been unsuccessful in predicting the performance of phase-change devices in the presence of fins and natural convection. This study presents a simplified numerical model based on a quasi-linear, transient, thin fin equation, which predicts the fraction of melted PCM, and the shape of the liquid–solid interface as a function of time with sufficient accuracy for engineering purposes. Experimental results are compared in dimensionless form with model predictions, and show fairly good agreement. To achieve high heat-transfer rates with a fixed amount of PCM and metal fin material, the model indicates that melting the PCM in a pure conduction mode with closely spaced thin fins is preferable to melting PCM with thicker fins spread further apart, even in the presence of natural convection.

NOMENCLATURE

<p>c_p, specific heat [kJ/kg °C];</p> <p>Fo, Fourier Number, $\frac{k_l t}{(\rho c_p)_l L^2}$;</p> <p>$g$, acceleration of gravity [m/s²];</p> <p>Gr, Grashof Number, $\frac{g \beta \Delta T L^3 \rho^2}{\mu^2}$;</p> <p>$h$, heat-transfer coefficient [W/m² °C];</p> <p>H, latent heat of fusion [J/kg];</p> <p>k, thermal conductivity [W/m °C];</p> <p>L, length [m];</p> <p>Nu, Nusselt number, hL/k;</p> <p>Pr, Prandtl number, $\mu c_p/k$;</p> <p>q, heat flow [W];</p> <p>Ra, Rayleigh number, $GrPr$;</p> <p>Ste, Stefan number, $\frac{C_{p1}(T_w - T_{m.p.})}{H}$;</p> <p>$t$, time [s];</p> <p>$T$, temperature [°C];</p> <p>V, volume [m³];</p> <p>x, distance in x-direction [m];</p> <p>y, distance in y-direction [m].</p> <p>$\%l$, volume fraction of melted PCM.</p>	<p>γ, $\frac{L_l}{L_c}$;</p> <p>γ_{lim}, γ convergence limit, $\frac{\gamma_{j+1} - \gamma_j}{\gamma_{j+1}}$;</p> <p>$\eta$, $\frac{x}{L_f}$;</p> <p>θ, dimensionless temperature, $\frac{(T - T_{m.p.})}{(T_w - T_{m.p.})}$;</p> <p>$\kappa$, $\frac{k_l}{k_m}$;</p> <p>λ, cell aspect ratio, $\frac{L_f}{L_c}$;</p> <p>μ, dynamic viscosity [kg/m s];</p> <p>ξ, $\frac{(\rho c_p)_m (T_w - T_{m.p.})}{H \rho_s}$;</p> <p>$\rho$, density [kg/m³];</p> <p>τ, dimensionless time, $\tau = \frac{k_m t}{(\rho c_p)_m L_f^2}$;</p> <p>$\psi$, $\frac{L_m}{L_c}$;</p>
---	--

Subscripts and superscripts

<p>Greek symbols</p> <p>β, thermal expansion coefficient [(°C)⁻¹];</p>	<p>c, cell;</p> <p>$cond.$, conduction;</p> <p>f, x-direction fin length;</p>
--	--

effort required to achieve a numerical solution of engineering accuracy. The two-dimensional limitation is not a serious restriction because practical systems will always require some depth to contain a sufficient volume of PCM to meet storage capacity requirements. Present experimental evidence shows that even with only 2.54 cm (1 in.) of depth the PCM melts almost completely in a two-dimensional fashion. The rest of the assumptions, outlined below, are based on physical arguments and experimental evidence, and are shown to be reasonably accurate over the range of intended use. The numerical model allows quantitative evaluation of the relative effects on melting rate due to fin thickness and length, distance between fins, physical properties of the PCM and fin material, and wall temperature boundary condition.

Assumptions

(i) The fin is sufficiently thin so that its temperature is considered to be a function of x -direction length only at any arbitrary time. For this assumption to be accurate, [17] states that:

$$\frac{k_m}{hL_m} > 6. \quad (1)$$

For the present application this condition is met, except during insignificant initial time periods when conduction across a very small liquid length (L_l) would impose comparatively large heat fluxes from the fin. Even while operating in the initial pure conduction mode in which $h = k_l/L_l$, assuming $k_m/k_l = 1000$, which is representative of PCM/metal combinations, and assuming $L_l/L_m = 0.01$, equation (1) becomes:

$$\frac{k_m}{hL_m} = \frac{k_m L_l}{k_l L_m} = 1000(0.01) = 10 > 6. \quad (2)$$

Hence, it is seen that except for a negligible initial time period during which $L_l/L_m \ll 1$, the thin fin assumption is indeed valid for representative PCM/metal combinations under practical consideration.

(ii) Heat conduction is neglected in the solid phase of the PCM. This assumption is exactly valid if the initial temperature of the storage cell is equal to the melting temperature of the PCM. In this case, any energy transferred to the solid will contribute only towards melting of the solid, and not towards conduction or sensible storage in the solid.

(iii) The principal mode of energy storage in a phase-change device is through latent heat of fusion effects. Therefore, sensible energy accumulation is neglected in both the liquid and solid phases of the PCM. For practical PCMs, $H/c_p > 100^\circ\text{C}$ [18]. Thus, for a 10°C operating range, sensible storage effects account for less than 10% of the total energy stored in the PCM. While sacrificing some absolute accuracy in accounting for this 10% of the total energy storage, this approximation allows a vast reduction of numerical effort which would otherwise be required to calculate the two-dimensional temperature distribution in the PCM. For more detailed heat transfer results, the

model could easily be modified to account for these sensible effects in a somewhat simplified fashion. For example, the fraction of sensible energy storage accumulated over a given time could arbitrarily be set equal to a fraction of latent heat storage predicted by the model at that same time. Although admittedly an approximate approach, this would increase the accuracy of the model for producing heat transfer information such as the average heat-transfer coefficient for the PCM cell.

(iv) All melting occurs on the y -direction face (the face which is perpendicular to the y -direction) of the PCM. An experimental comparison between a finned and an unfinned PCM cell, which is discussed in greater depth in the Results and Discussion section, shows that after a short initial time period the fins play a dominant role in determining the shape of the melting profile. The validity of this assumption depends on the cell aspect ratio λ , the ratio of fin length to distance between fins. A long fin will have more effective heat-transfer surface than a shorter fin to melt the PCM on its y -direction face for a fixed amount of heat transfer surface to melt on the x -direction, or normal face.

(v) Physical properties for the PCM liquid phase, the PCM solid phase and the metal fin are assumed to be constant. Rigorously, physical properties vary with temperature; however, for the relatively small temperature differences typical of PCM storage devices the variations are insignificant. It should be noted that the model does assume different densities for the solid and liquid PCM phases. Data for n -octadecane [16], the PCM used in the present experimental study, show that over the largest temperature range examined experimentally (20°C), ρ_l varies less than -2% , c_{pl} varies less than $+2.5\%$ and k_l varies between -8.5% and $+2.6\%$. The variation in k_l is due to the spread of data given for k_l which is probably from several different sources.

Model equations

An energy balance conducted on an arbitrary differential element dx , shown in Fig. 2(b), using the assumptions discussed above, yields two equations which are the basis for the model. First, examine the metal fin, for which:

$$q_{f-\text{sens.}} = q_{\text{cond. (net)}} + q_{f-\text{PCM}}. \quad (3)$$

This equation can be rewritten more specifically as:

$$(\rho c_p)_m L_m \frac{\partial T}{\partial t} = k_m L_m \frac{\partial^2 T}{\partial x^2} - h(T - T_{m.p.}), \quad (4)$$

where T is the fin temperature, which is a function of fin length and time.

The sensible energy term for the fin in equation (4), $(\rho c_p)_m L_m \partial T/\partial t$, is included only to determine the temperature distribution along the fin, which significantly affects the melting rate. The contribution of sensible energy storage in the fin on the total energy in the PCM cell is negligible and therefore is not included. As mentioned in assumption (iii), the model

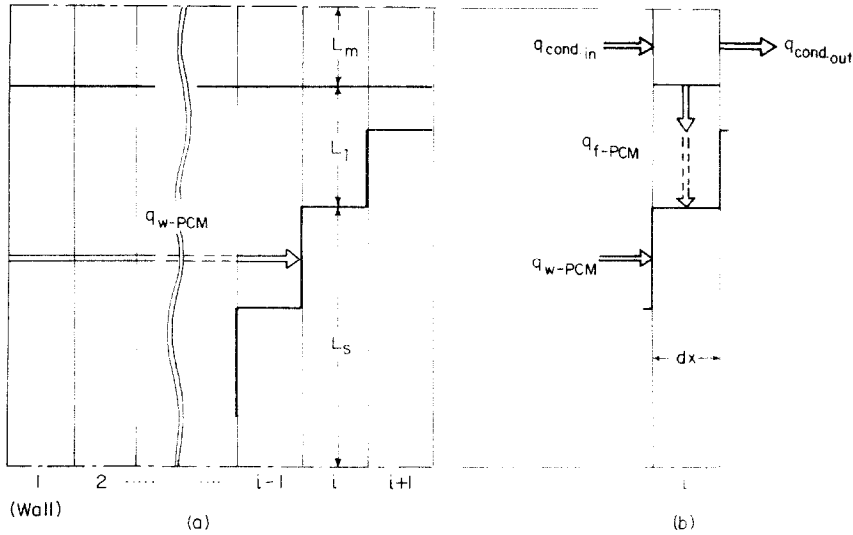


FIG. 2(a). A representation of the discrete system in which L_i is allowed a continuous value at each node. (b). Energy fluxes on an arbitrary slice of the symmetry cell.

is presently set up so that the heat-transfer rate is directly proportional to the melting rate, and sensible effects are not included.

Melting of the PCM proceeds due to energy transferred from two distinct sources, the fin and the constant temperature end wall. Heat transfer from the fin is given by

$$q_{f-PCM} = h(T - T_{m.p.})dx, \quad (5)$$

where h , the heat-transfer coefficient between the fin and the solid PCM, is determined as discussed in a following sub-section. In the actual melting process heat from the fin causes melting primarily on the y -direction face of the solid. Heat transferred from the constant temperature end wall, q_{w-PCM} , is determined from pure conduction through the liquid in the x -direction:

$$q_{w-PCM} = \frac{k_l}{x}(T_w - T_{m.p.}) \frac{\partial L_i}{\partial x} dx. \quad (6)$$

Equation (6) is a first order approximation, accounting for x -direction conduction only of the amount of heat which causes melting on the x -direction face of the solid. This simplification leads to inaccuracies in the model predictions in regions close to the constant temperature wall (small x). Convective effects on q_{w-PCM} were not taken into account due to the relatively small influence of these effects on the overall performance of cells with large λ , for which this model was designed. An accurate prediction of convective terms here would require convection to increase as the PCM has melted away from the wall, and then decrease after a sufficient amount has melted. This decrease is due to a reduction of the temperature gradient between the fins as their effect on the PCM becomes dominant. q_{w-PCM} is dominant during the very early stages of melting before sufficient energy has

diffused through the fin to provide an appreciable amount of q_{f-PCM} , which subsequently becomes the dominant source of heat for melting. It should be noted that q_{w-PCM} is the only source of heat in an unfinned PCM device.

Assumption (iv) states that all melting is to take place on the y -direction face of the solid. To implement this assumption the sum of q_{f-PCM} and q_{w-PCM} is the quantity of heat which is used to recede the liquid–solid interface in the y -direction at every point along the interface. Thus the second equation, which determines the rate of interface recession and hence, the interface position, is given by:

$$H\rho_s \frac{\partial L_i}{\partial t} = h(T - T_{m.p.}) + \frac{k_l}{x}(T_w - T_{m.p.}) \frac{\partial L_i}{\partial x}. \quad (7)$$

Dimensionless groups and the dimensionless equations

Equations (4) and (7), the model differential equations, are converted into dimensionless form by using the dimensionless variables $Nu_c, \eta, \lambda, \gamma, \psi, \kappa, \theta, \tau$ and ξ , as defined in the nomenclature.

Note that τ is similar to the Fourier number Fo ; however, time is normalized with respect to the metal fin properties to allow easy comparison between prospective PCM's for otherwise identical systems. ξ is a modified Stefan number Ste . Equation (4), rewritten in dimensionless form, determines the dimensionless temperature distribution along the fin:

$$\frac{\partial \theta}{\partial \tau} = \frac{\partial^2 \theta}{\partial \eta^2} - \frac{\lambda^2 \kappa Nu_c}{\psi} \theta. \quad (8)$$

Equation (7), rewritten in dimensionless form, determines the dimensionless rate of liquid–solid interface recession as a function of dimensionless length along the fin:

$$\frac{\partial \gamma}{\partial \tau} = \xi \kappa \left[\lambda^2 Nu_c \theta + \frac{1}{\eta} \frac{\partial \gamma}{\partial \eta} \right] \quad (9)$$

Determining the heat-transfer coefficient for q_{f-PCM} in equation (5)

A heat-transfer coefficient h as defined by equation (5) is required to calculate the heat flux in the y -direction from the fin to the PCM. For a horizontal fin geometry with relatively small spacing between fins, conduction is the primary mode of heat transfer. Natural convection may be present due to fluid instabilities both above and below a fin. Instabilities above a fin are created because the bottom surface of the relatively cool liquid–solid interface is oriented above the warmer fin surface. Instabilities below a fin arise as cool fluid flows down along the incline of the top surface of the liquid–solid interface. Although convection has the effect of destroying the symmetry present in pure conduction melting, the present experimental work has shown that the melting interface is still approximately symmetric. This suggests that convective effects are of secondary importance in this geometry, and that they are approximately equal both above and below a fin. Nevertheless, buoyant effects must be included to achieve a prediction of engineering accuracy when they are present. This is accomplished through the use of a simple Nu vs Ra correlation:

$$Nu = 1, Ra \leq \text{Rayleigh stability limit} \quad (10a)$$

$$Nu = A Ra^n, Ra > \text{Rayleigh stability limit}, \quad (10b)$$

where A and n are correlation coefficients determined by experiments conducted for a particular geometry. In the present system a large portion of the unstable region is similar to two horizontal parallel plates, a distance L_1 apart. Hence, for a differential element dx , a correlation was sought for:

$$Nu = \frac{hL_1}{k_l} \text{ vs } Ra = \frac{g(T - T_{m.p.})\rho_l^2 c_{pl} L_1^3}{\mu k_l} \quad (11)$$

Investigations have been conducted to determine the relationship between Nu and Ra for horizontal parallel plates [19]. However, several complications arise which must be considered before applying such a correlation to the present application.

The majority of the data have been presented for steady state heat transfer between stationary plates when the spacing between plates is much smaller than their dimensions. Neither of these conditions are met in the present system. Boger and Westwater [20] have examined buoyancy in ice–water phase-change systems and have concluded that, for their case, the interface motion was slow enough to consider the system as quasi-steady so that steady state relations could still be applied successfully. Also, in the present work dx is not greater than L_1 ; hence, the available correlations are again questionable. Catton and Edwards [21] examined the effects of both conducting and non-conducting side walls on natural convection between two horizontal surfaces and concluded that for aspect ratios (distance between plates/plate length) greater than 0.5, the side walls have the effect of reducing Nu for a given Ra due to two effects. First, the

side walls slow down the flow which reduces heat transfer and, second, the walls tend to conduct heat and, therefore, reduce temperature gradients in the fluid. This results in an increase of the Rayleigh stability limit. The normal Rayleigh stability limit for horizontal parallel plates without any wall effects is about 1700. This was the value used throughout the present numerical study. In the present system it was not the side walls which reduced natural convection, but the influence of the flow in neighboring differential elements. Through continuity and viscous shear, flow in one differential element was reduced by a reverse flow or stagnant region nearby. For this reason a standard correlation for horizontal parallel plates will overpredict the heat transfer coefficient for the present geometry.

A correlation of:

$$Nu = 1, (Ra \leq 1700) \quad (12a)$$

$$Nu = 0.4753 Ra^{0.1}, (Ra > 1700) \quad (12b)$$

was used throughout the numerical study. The correlation coefficients were determined by trial and error to agree with the data for one experimental run conducted with parameters at approximately mid-range values. These same coefficients were then applied identically to all the numerical predictions. Further optimization of this correlation was not necessary as it provided reasonable accuracy over the entire parameter range studied in the experiments. Finally, Nu is converted to Nu_c for use in the equations via:

$$Nu = \frac{Nu_c}{\gamma + L_{cond.}} \quad (13)$$

$L_{cond.}$ is a conduction length parameter required to avoid singularities associated with startup conditions. A value of $L_{cond.} = 0.22$ was used throughout the numerical study. This value was determined by comparing model predictions with experimental data for the initial conduction regime of the above intermediate-range experimental run.

The discretized equations and numerical solution method

Equations (8) and (9) were discretized to their finite difference forms and a Fortran computer code* was developed to solve them. Figure 2(a) gives a representation of the discretized geometry. Since temperature variations are neglected in the original PCM, the liquid–solid interface profile and the temperature along the fin can be determined using a spatially one-dimensional (η) set of nodes. The value of γ at each node is allowed to vary continuously rather than be constrained to certain discretized values as it would be in a spatially two-dimensional grid model. This procedure offers the advantages of both reducing the numerical effort required to achieve a solution while yielding a more continuous determination of interface

* Available on request.

profile than is possible with a corresponding spatially two-dimensional numerical grid.

Equation (8) was discretized as follows:

$$\frac{\theta_{i,j+1} - \theta_{i,j}}{\Delta\tau} = \frac{\theta_{i+1,j+1} - 2\theta_{i,j+1} + \theta_{i-1,j+1}}{(\Delta\eta)^2} - \frac{\lambda^2 \kappa N u_{c,i,j}}{\psi} \theta_{i,j+1}. \quad (14)$$

Equation (14) is a fully time-implicit approximation. This was used to ensure stability in the calculation procedure. A spatial central difference formulation, with error of order $(\Delta\eta)^2$ was used to approximate $\partial^2\theta/\partial\eta^2$. The time derivative $\partial\theta/\partial\tau$ was approximated by a forward difference with an error of order $\Delta\tau$. Equation (14) leads to a tridiagonal system of simultaneous equations which were solved with a tridiagonal matrix algorithm [22] using gaussian elimination.

Equation (9) was discretized as follows:

$$\frac{\gamma_{i,j+1} - \gamma_{i,j}}{\Delta\tau} = \zeta \kappa \left[\lambda^2 N u_{c,i,j} \theta_{i,j+1} + \frac{1}{(i+0.5)\Delta\eta} \frac{\gamma_{i+1,j} - \gamma_{i-1,j}}{2\Delta\eta} \right]. \quad (15)$$

Again, a forward difference approximation was used for the time derivative term, $\partial\gamma/\partial\tau$. The length derivative $\partial\gamma/\partial\eta$ was approximated by a central difference which has an error of order $(\Delta\eta)^2$. The equation system was quasi-linearized by solving for $\theta(\eta, \tau)_{j+1}$ from equation (14). These values were then used to determine the new interface position $\gamma(\eta, \tau)_{j+1}$ from equation (15) and the new values of γ were used to determine a more accurate Nu_c in equation (14). This process was iterated until γ converged to within a predetermined convergence limit (γ_{lim}) everywhere in the phase-change system. Once γ had converged, equation (14) was solved again and the solution procedure advanced to the next time level ($j+2$).

The numerical procedure was run on a CDC 6400 computer system. No practical restrictions were found constraining the sizes of $\Delta\tau$ and $\Delta\eta$ to ensure stability due to the fully implicit formulation of equation (14). A sensitivity study was performed on one particular test run to determine the effects of various values for $\Delta\tau$, $\Delta\eta$ and $\gamma_{lim} = 0.01$. The numerical predictions presented were run using $\Delta\eta = 0.05$, $\Delta\tau = 0.1$, $\gamma_{lim} = 0.01$. The predictions presented here varied less than 2% from the most refined predictions calculated which used values of $\Delta\eta = 0.01$, and $\Delta\tau = 0.01$. Central processor time required for the reported results varied between 10 and 50 s depending on the real time duration required to achieve complete melting of the PCM. This is in contrast to CPU times of 15 min to 1 h required by the spatially two-dimensional numerical grid conduction model reported by Humphrey [15] and is seen to be a major advantage of the model in the present work. The FORTRAN Program required less than 40k octal words to load and execute with a maximum

refinement of 201 nodes ($\Delta\eta = 0.005$).

EXPERIMENTAL APPARATUS AND PROCEDURE

A series of experiments were conducted to test the validity of the model for various values of θ and ξ (via $T_w - T_{m,p}$) and ψ (via L_m). The apparatus was composed of several components including a two-cell test section, a temperature controller for the test section wall heater, instrumentation and a constant temperature air bath environment.

Apparatus

The principal components of the apparatus shown in Fig. 3, consisted of two aluminum fins with PCM in between in a Plexiglas enclosure of inside dimensions $12.70 \times 2.54 \times 3.18$ cm ($5 \times 1 \times 1.25$ in). A two-fin test section was used to ensure symmetry effects found in a larger device. One end of the container was insulated, which the other end consisted of an electrically heated aluminum plate with a thickness of 6.4 mm (1/4 in). To insure good thermal contact between the fins and the plate, Wakefield thermal compound ($k = 0.787$ W/m $^\circ$ C [0.454 Btu ft h $^\circ$ F]) was applied to the ends of the fins, which were spring-loaded against the plate. The side walls were left uninsulated to allow visual observation of the melting process. The 6.4 mm (1/4 in) Plexiglass walls acted as sufficient insulation to prevent significant heat loss to the environment. This was evidenced by a primarily two-dimensional melting process which showed no wall effects.

The aluminum end plate was heated with a 3.81×4.45 cm (1.25×1.75 in) Minco Thermofoil heater (120 Ω), which was insulated from behind. The heater was bonded to a 1.6 mm (1/16 in) thick aluminum plate with silicone adhesive provided with the heater. This thin aluminum plate was then joined to the 6.1 mm (1/4 in) thick aluminum end plate with thermal compound. A temperature controlling circuit was designed and built to control the Minco Thermofoil heater, and thus provide a constant end plate temperature during the course of a run. After the initial transient preceding the final set temperature, the plate temperature remaining constant within $\pm 0.25^\circ$ C was typically within $\pm 0.50^\circ$ C. The time required to reach steady state temperature was a function of $(T_w - T_{m,p})$; for $\Delta T = 20^\circ$ C, $t \approx 12$ min, or $\tau \approx 3.8$. This was more than twice as long as the next longest startup time, and was the only case where the startup time was more than 5% of the total run time.

Temperature was monitored using 8 Omega 24-gauge iron-constantan thermocouples. Of these 8 thermocouples, three were mounted on the test section itself; one in the aluminum end plate close to the PCM, one behind the thermofoil heater and one at the insulated end of the container. The remaining thermocouples were located in the constant temperature air bath.

All experiments were conducted in a constant temperature air bath environment set 1° C below the

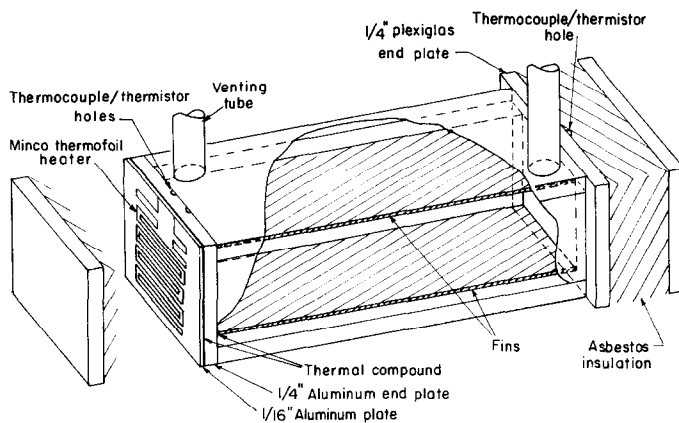


FIG. 3. Experimental test section.

melting point of the PCM. This was done to enforce the condition of negligible thermal conductivity in the solid phase of the PCM; i.e. all of the energy transferred to the solid phase contributed only towards melting the solid, and also minimized heat loss from the experiment to the environment.

n-Octadecane, $\text{CH}_3(\text{CH}_2)_{16}\text{CH}_3$ (97% pure), was used exclusively as the PCM in the experiments. It is a desirable compound to use in experimentation because of its relatively low and uniform melting point (28°C), and the fact that it exists as a single phase in the solid state. Material properties for *n*-octadecane are listed in Table 1. Expansion due to the density differences of the two PCM phases was handled by allowing a small excess of liquid PCM to escape through vent tubes provided in the test section. The *n*-octadecane was degasified during the freezing process by vibrating the test section on a high frequency shaker table while controlling the rate of freezing.

Procedure

Eleven runs were conducted to study the effects of changing wall temperature T_w (or ξ) and fin thickness L_m (or ψ). Table 2 lists the parameters used for each run. The two-cell test section was placed in the air bath until its temperature leveled off at 27°C . Then the heater was switched on and photographs were taken at recorded times to establish the interface profiles. Melt fraction was determined by measuring the solid or liquid areas on each photograph with a polar planimeter. The absolute error and standard deviation of these measurements was kept below 1%.

RESULTS AND DISCUSSION

Figures 4 and 5 show photographic sequences illustrating the shape of the liquid–solid melting interface with and without fins. The solid PCM appears white or gray, and (because of the background) the liquid PCM is black. It should be noted

Table 1. Physical properties of *n*-Octadecane and Aluminum (references given in brackets, A denotes reference from the Aldrich Chemical Company)

Property	SI Units	English units
<i>n</i> -Octadecane:		
ρ_l [A]	777.0[kg/m ³]	48.51[lbm/ft ³]
ρ_s [17]	852.8[kg/m ³]	53.24[lbm/ft ³]
k_l [12]	0.149[W/m °C]	0.086[Btu/ft hr °F]
c_p [12]	2.66[kJ/kg °C]	0.64[Btu/lbm °F]
μ_l [17]	3.8×10^{-3} [kg/m s]	9.19[lbm/ft hr]
H [12]	241.36[kJ/kg]	103.81[Btu/lbm]
β [17]	1×10^{-3} [1/°C]	1.8×10^3 [1/°C]
6061 T4 Aluminum:		
ρ_m [26]	2712.6[kg/m ³]	169.3[lbm/ft ³]
k_m [26]	179.962[W/m °C]	104.0[Btu/ft hr °F]
c_{p_m} [26]	0.96[kJ/kg °C]	0.23[Btu/lbm °F]

Table 2. Experimental runs and relevant parameters; for all runs: $L_f = 5$ in., $L_c = 0.625$ in., $\lambda = 8$, $\kappa = 8.28 \times 10^{-4}$ (except run No. 10, where $L_c = 0.594$ in., and $\lambda = 8.4$)

Run No.	L_m (in.)	ψ	$(T_w - T_{m.p.})$	ξ
1	0.125	0.20	20°C	0.2530
2	0.125	0.20	20°C	0.2530
3	0.125	0.20	10°C	0.1265
4	0.125	0.20	5°C	0.0633
5	0.125	0.20	15°C	0.1898
6	0	0.0	10°C	0.1265
7	0.0625	0.10	10°C	0.1265
8	0.0625	0.10	15°C	0.1898
9	0.09375	0.15	10°C	0.1265
10	0.09375	0.16	10°C	0.1265
11	0.09375	0.15	15°C	0.1898

that time in the figures is normalized by the same conversion factor, so the time response of the different runs may be compared directly. Complete tabulations of the data corresponding to all the experimental runs may be found in Henze [24].

The effect of fins on the interface shape and melting rate

Figure 4 shows the melting interface for $\Delta T = 10^\circ\text{C}$ for the case with no fins. This run was carried out to provide a reference for comparison with the finned runs. Two basic melting regimes were present: conduction from the wall early in the melting process [before photograph (a)], followed by natural convection arising from fluid instabilities, which has just begun prior to photograph (a). In the first regime, the entire interface recedes uniformly in the x -direction normal to the constant temperature wall, except for two small regions at the top and bottom of the container. In these regions, the Plexiglas container itself acts as a fin because the conductivity of the Plexiglas is greater than that of the PCM. This causes slightly faster melting in these two regions. The effect is only apparent at the bottom of the interface in Fig. 4 (a–f) because at the top natural convection has caused it to melt away. Once the distance between the interface and the constant temperature wall is large enough, natural convection is initiated as liquid starts to flow up along the heated wall. The liquid is redirected by the top of the container, causing it to impinge on the upper portion of the interface which results in significantly faster melting of the upper portion, as is apparent in Fig. 4 (a–f).

Figure 5 shows the melting interface for a typical experimental run with fins. The photographic sequence illustrates the dominating influence that the fins have on the shape of the melting interface. In contrast to the unfinned case in Fig. 4, the interfaces in the finned runs were always approximately symmetric, with a large portion of PCM melting away from the

fins, almost parallel to the fin surfaces. There are three regimes of melting in the finned runs; pure conduction from the constant temperature wall and the fins, conduction from the fins with some natural convection from the end wall, and finally, natural convection from the fins.

Pure conduction is illustrated in the photograph (a) of the sequence in Fig. 5 and is evidenced by a symmetric interface shape and fairly sharp corners on the left-hand side of the interface. Even for these early time stages, an appreciable percentage of the melted PCM is due to the fin, as some liquid is present along most or all of the fin length. Convection from the end wall, similar to that present in the unfinned run, then causes the top left end of the interface to recede slightly faster than the bottom. This is illustrated most strongly in photographs (b) and (c) of the sequence. At this time, the interface is the least symmetric. The presence of the fins tends to decrease temperature gradients in the liquid and, hence, reduce natural convection from the end wall in regions where no solid PCM is present (regions to the left-hand edge of the interface). Therefore, as time progresses, convection from the end wall decreases. As this happens, the interface continues to recede further from the fins as a result of conduction from the fins, which finally leads to natural convection from the fins. This acts to return symmetry to the interface shape in the remaining stages of melting (photographs d–f).

Below the interface, free convection is due to the instability induced in the fluid by the hot fin positioned below the cold interface. The lower surface of the melting interface tended to be significantly more irregular than the top surface, particularly in regions where L_f was larger and in runs with higher temperature differences ($T_w - T_{m.p.}$), hereafter referred to as ΔT . This irregularity is postulated to arise from circulation patterns produced by small convective cells (Bernard cells) which arise due to free convection below the interface. Once established, the irregularities appeared to channel the flow of the cells causing them to be further accentuated. The irregularity locations can be seen most clearly in sequence (c–f) of Fig. 5 and always appeared to be fairly periodic. Their presence progressed to the right (larger x) as time increased, because L_f became large enough to cause Ra to increase beyond its stability limit. It was verified that small amounts of air trapped in the PCM were not the cause for the irregularities.

Convection above the liquid–solid interface is due to cool fluid flowing down the inclined interface (to the left in the photographs). This causes the top surface of the interface to be very smooth due to the melting away of any irregularities. Flow visualization experiments would be very useful in helping to obtain detailed information as to the direction and magnitude of convective effects in various locations and at various times during the experiment. The photochromic flow visualization technique described in reference [25] would be especially well-suited to the present

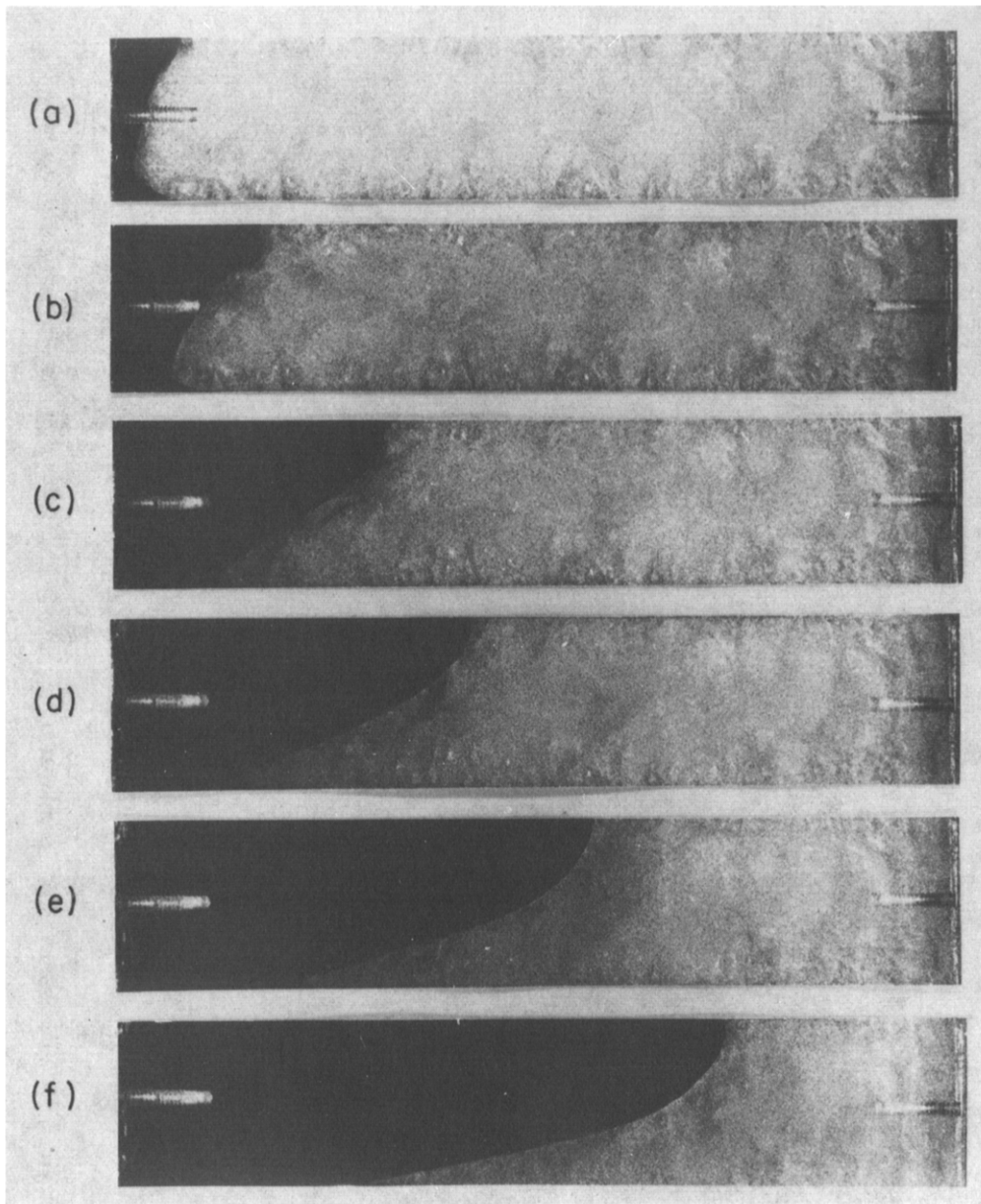


FIG. 4. Liquid–solid interface for run No. 6, no fins, $\Delta T = 10^\circ\text{C}$; (a) $\tau = 8.40$, $\%l = 4.9$; (b) $\tau = 22.30$, $\%l = 12.0$; (c) $\tau = 46.75$, $\%l = 23.1$; (d) $\tau = 65.48$, $\%l = 31.0$; (e) $\tau = 99.71$, $\%l = 43.8$; (f) $\tau = 148.02$, $\%l = 59.4$.

application.

Figure 6 is a plot of some experimental results. The random errors involved with the measurements of τ and $\%l$ or melt fraction, are stated in the experimental section and are within the size of the plotted symbols. A systematic error involved in the measurement of the temperature in the constant temperature end wall may be present in some runs, causing a bias in those data curves. This would be responsible, for example, for the difference between run No. 1 and run No. 2 which should have been identical. Although these two runs are fairly close, it appears that run No. 1 was systematically biased with a ΔT about 1°C lower than run No. 2.

Figure 6 shows that the presence of fins significantly increases the overall heat transfer to, and melting of, the PCM. Both of the finned runs at 10°C had a melting rate of 400% that of the unfinned run for 10°C . The effect of ΔT on the melting rate was much more significant than the effect of L_m in the parameter range examined in the experiments. For a given fin thickness, doubling ΔT approximately doubled the melting rate. It should be noted from the dimensional analysis presented in the model section, that doubling the latent heat of fusion H would have an effect equal to that of halving ΔT . Changing L_m from $1/8$ to $1/16$ in. reduced the melting rate by approximately 15%.

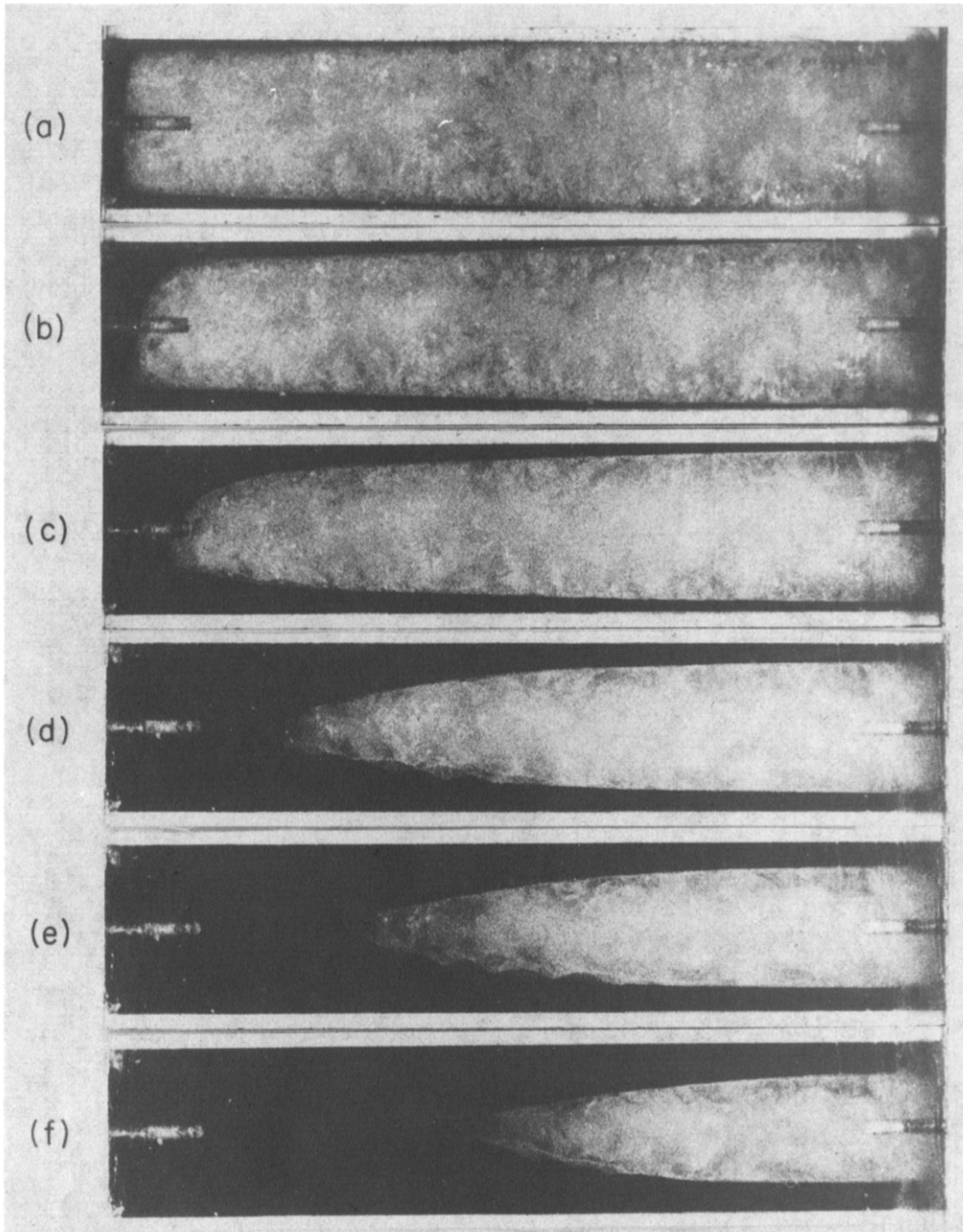


FIG. 5. Liquid-solid interface for run No. 10, $L_m = 3/32$ in, $\Delta T = 10^\circ\text{C}$: (a) $\tau = 3.35$, $\%I = 7.6$; (b) $\tau = 7.94$, $\%I = 15.5$; (c) $\tau = 14.81$, $\%I = 27.2$; (d) $\tau = 29.89$, $\%I = 46.6$; (e) $\tau = 37.72$, $\%I = 57.4$; (f) $\tau = 47.41$, $\%I = 69.0$.

Comparison of model predictions and experimental results

Figure 7 shows typical interface shapes predicted by the model corresponding to some of the experimental runs performed. The predictions are plotted with their shape symmetric about the top axis of the plots. The six lines plotted depict the interface position at various values of τ .

The model predictions of interface position, although qualitatively correct in predicting the relative differences between the shapes, are somewhat deficient due to the simplicity of the model. The melting

interface does not recede from the constant temperature end wall as much as it should. This is due primarily to the method of determining $q_w - \text{PCM}$ and the assumption that all melting occurs through the y -direction face of the PCM. The experiments are a rigorous test of the model because the cell aspect ratio λ is fairly low. For a greater value of λ , one could expect a significant improvement in the model predictions of interface shape. The model is much more successful in predicting the percent of melted PCM ($\%I$), or melt fraction, as a function of τ .

Figure 8 compares model predictions (shown by

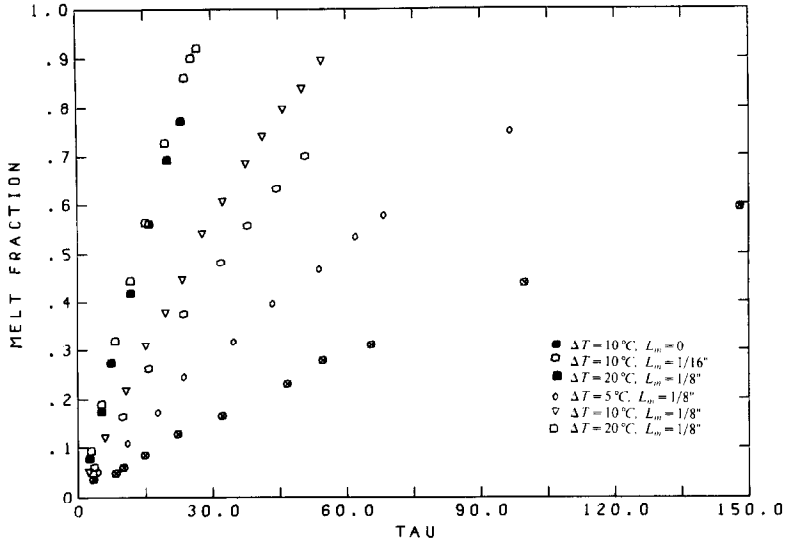


FIG. 6. Melt fraction of PCM vs τ for several experimental runs.

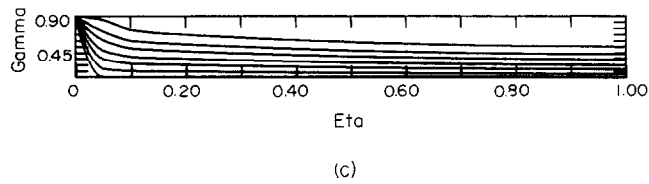
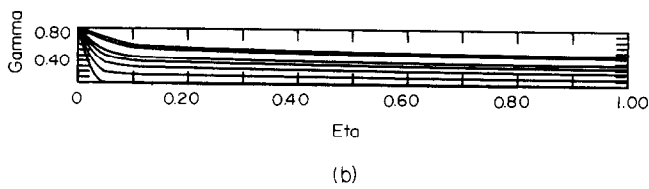
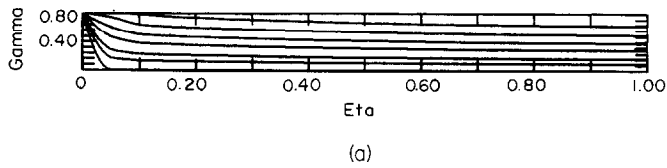


FIG. 7. Model predictions of the lower symmetric half of the liquid–solid interface locations for: (a) $L_m = 0.125$ in., $\Delta T = 10^\circ\text{C}$, $\tau = 6, 11, 20, 28, 38, 50$; (b) $L_m = 0.125$ in., $\Delta T = 5^\circ\text{C}$, $\tau = 11, 24, 35, 43, 62, 68$; (c) $L_m = 0.0625$ in., $\Delta T = 10^\circ\text{C}$, $\tau = 4, 10, 16, 24, 32, 44$.

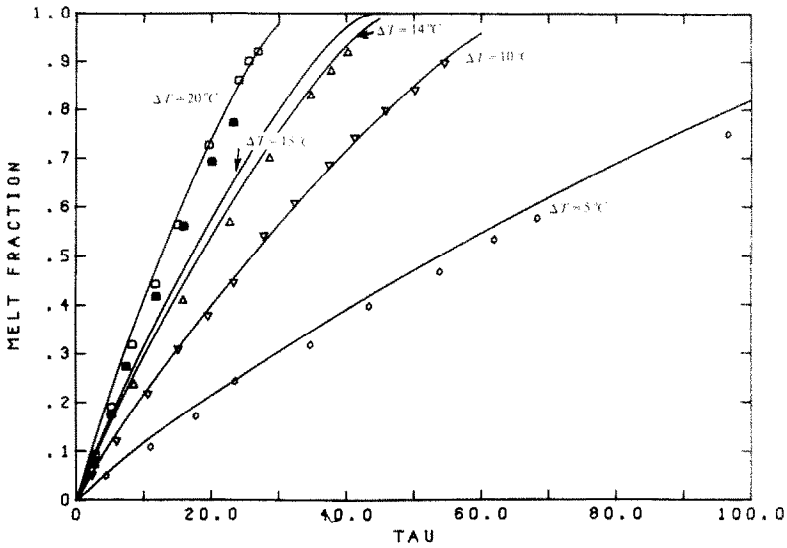


FIG. 8. Comparison of model predictions (—) and experimental results for melt fraction vs τ for $L_m = 0.125$ in., and various ΔT 's.

lines) with experimental data for $L_m = 1/8$ in. and various ΔT 's. The model is very successful in predicting quantitatively the effects of different ζ 's (in this case caused by different ΔT 's). Again, a possible systematic bias in the experimental constant wall temperature could explain the spread in the two 20°C runs. It is shown that a prediction for an otherwise identical run with $\Delta T = 14^\circ\text{C}$ shows better agreement with the experimental data for $\Delta T = 15^\circ\text{C}$.

Figure 9 gives a comparison for runs with $\Delta T = 10^\circ\text{C}$ and different values of L_m . The data for no fins is also provided as a reference. Figure 10 is a similar plot for the three L_m 's with $\Delta T = 15^\circ\text{C}$. The effect of L_m in the range examined experimentally was fairly small.

However, the model appears to predict the $L_m = 0.125$ in. and $L_m = 0.0625$ in. cases fairly well. Because the system is much more sensitive to $\Delta T(\zeta)$ than it is to $L_m(\psi)$, a comparison for $L_m = 0.09375$ in. is difficult to make in both the 10 and 15°C run cases due to possible experimental temperature biases. A 1°C bias in the constant end wall temperature was shown above to have a significant enough effect to cause the discrepancies. Physically, the model results make more sense than the experimental data, particularly for $L_m = 0.09375$ in. with $\Delta T = 10^\circ\text{C}$, where the data practically falls on the $L_m = 0.0625$ in. run. Intuitively, this run would be expected to fall between the 0.125 and 0.0625 in. cases, as the model predicts.

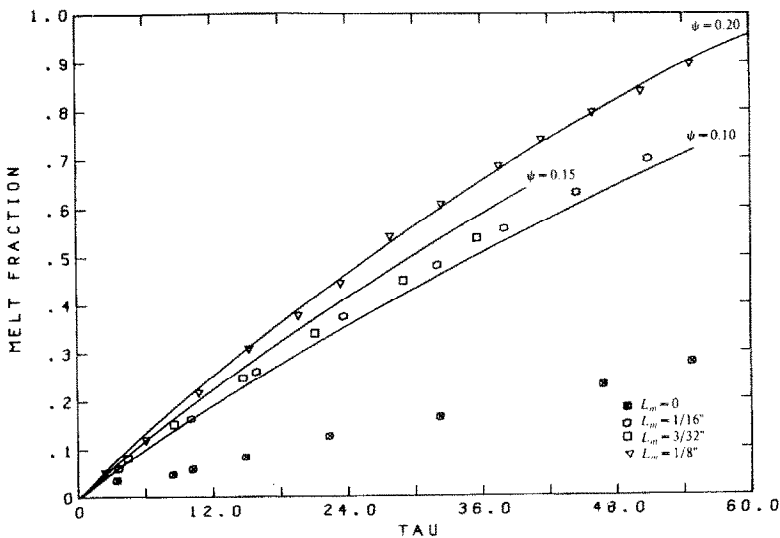


FIG. 9. Comparison of model predictions (—) and experimental results for melt fraction vs τ for $\Delta T = 10^\circ\text{C}$, and various L_m 's.

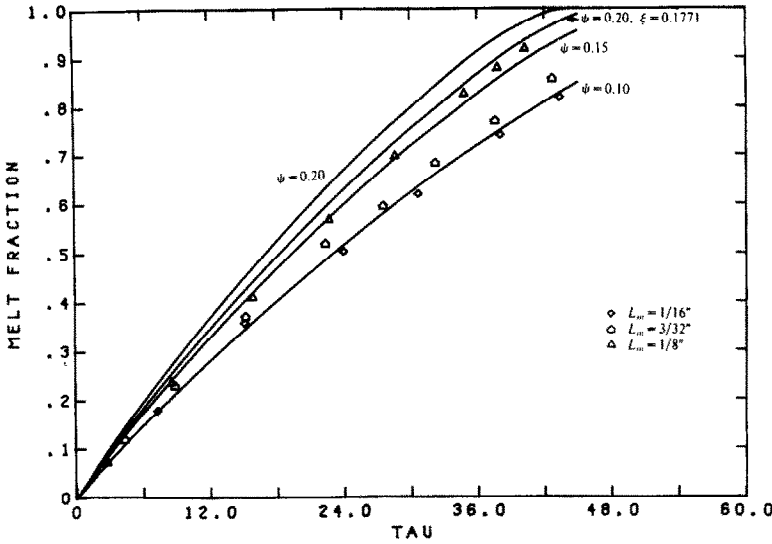


FIG. 10. Comparison of model predictions (—) and experimental results for melt fraction vs τ for $\Delta T = 15^\circ\text{C}$, and various L_m 's.

Applications of the model

For the horizontally finned geometries considered in this study, the magnitude of heat transfer due to natural convection depends on L_c , L_m and ΔT , the parameters which influence Ra . An example of the magnitude of these effects on the melting rate for $L_m = 0.125$ in., and $\Delta T = 5, 10$ and 20°C , as predicted by the model is shown in Fig. 11. For each of the three cases the upper curve is the natural convection result which agrees with the experimental data as shown in Fig. 8. The lower curves are the model predictions for pure conduction only for the same 3 runs. These are

calculated by artificially setting the value for the Rayleigh stability limit greater than the value of the cell Rayleigh number in the input to the model. As expected, the magnitude of the melt fraction due to convection is larger for the larger temperature differences.

The model can be used to aid in the design process for a finned PCM device. Based on design requirements such as total storage capacity, heat-transfer rates, costs for PCM and metal fins and manufacturing limitations, the model can be used to predict the most efficient and economical geometric configuration for L_c , L_m and L_f .

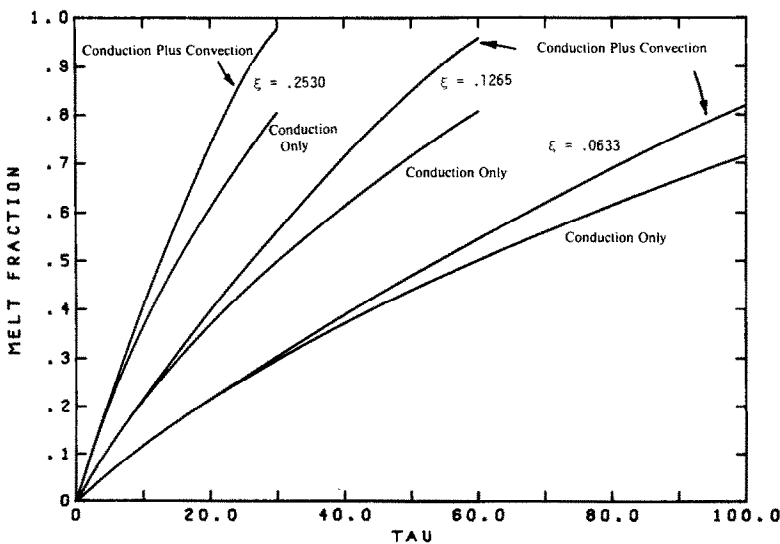


FIG. 11. Model predictions of conduction only (lower curve), and conduction plus natural convection (upper curve) for various ξ 's.

Given a fixed amount of fin material and PCM, would it be more advantageous to: (a) have the fins further apart (larger L_c) and benefit from increased convection effects; (b) have thinner fins spaced closer together; (c) have thinner fins which are longer and spaced at a larger L_c ? The answer to this question is based on many factors, and can be predicted by the model. For a fixed amount of PCM and fin material, and a fixed L_f , Fig. 12 shows predictions for conduction only and conduction plus convection for 3 cases with the same ΔT . The slowest melting rate is for $\psi = 0.2$, $\lambda = 8$, which is identical to the experimental case with $\Delta T = 10^\circ\text{C}$ and $L_m = 0.125$ in. The second and third sets of curves correspond to conduction only and conduction plus convection with $\psi = 0.2$, $\lambda = 16$ and 32, respectively. These last two cases correspond to fins that are half as thick, with half the spacing between fins as each previous run. The model indicates that the magnitude of convective effects decreases for the higher λ cases due to a decrease in L_c (or more accurately $L_c - L_m$). For the $\lambda = 32$ case, convection has no effect on the melting rate of the system, and the two curves fall on top of each other. This indicates that to achieve high heat transfer rates for a given L_f and ΔT , it is advantageous to use thinner, more closely spaced fins, even though this acts to decrease the effects of convection. When the fins are spaced closely enough, which the model indicates to be an advantageous situation, natural convection effects arising from fin orientation, horizontal or otherwise, become negligible. In such cases, when melting occurs in a pure conduction mode, the model can be used to predict melting in a PCM cell with any direction of fin orientation with a high degree of accuracy.

CONCLUSIONS

A simplified model based on a transient, quasi-

linear, thin fin equation was developed to predict the melting interface profile and the fraction of melted PCM as a function of time. A series of experiments which varied ξ and ψ , the dimensionless driving force and fin thickness parameters, respectively, were conducted to validate the model.

The model was proven to be fairly successful in quantitatively predicting the melt fraction of PCM vs time for both of these effects. Because the system was more sensitive to changes in ξ , a possible systematic bias of the end wall temperature in some of the experimental runs made the effects of different ψ 's difficult to determine for the intermediate value of $\psi = 0.15$. This does not necessarily reflect an inadequacy of the model, which agreed with the experimental data for the two extremes of ψ , and predicted an appropriate melting rate of the melting interface.

Model predictions of the melting interface profiles, although qualitatively correct in identifying differences between the runs, are inadequate for providing accurate details of the receding interface. This is largely due to the simplicity of the model, specifically in the determination of q_{w-PCM} in equation (6), and the assumption that the PCM melts only through its y-direction face. This assumption, however, does allow a very large reduction in the CPU time required for the model to achieve a solution, from 15–60 min for a spatially two-dimensional grid model [15–16], to 10–15 s for the present model. Predictions of melting profiles are substantially more accurate for larger cell aspect ratios, λ .

The model is useful for determining the most efficient and economical geometric configuration in a finned PCM device after accounting for other design constraints. It should be noted that a similar analysis could be carried out for the freezing process, where a finned geometry would have an even greater advantage over an unfinned device due to the reduced

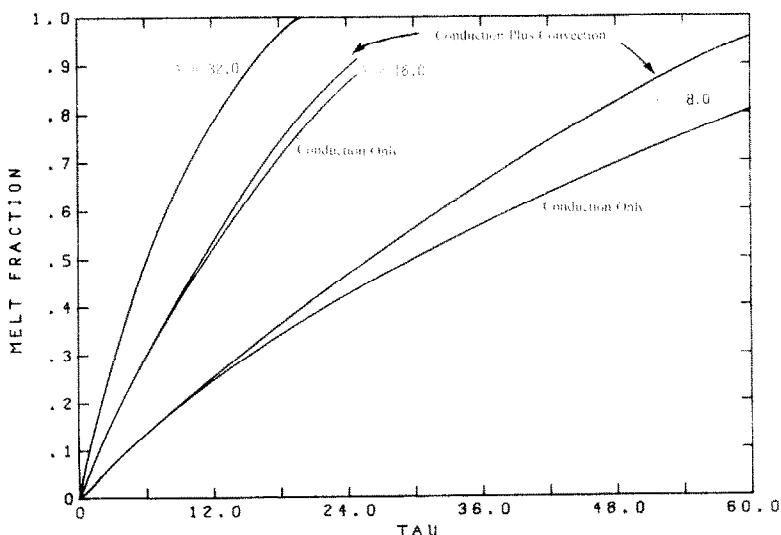


FIG. 12. Model predictions of conduction only, and conduction plus natural convection for $\lambda = 8, 16, 32$.

convective effects present during the freezing process.

Acknowledgements—We would like to thank Professor Alan Laird for his interest and encouragement during the course of this investigation and the Seawater Conversion Laboratory of the University of California Water Resources Center, who provided the financial support to make this project possible. Computational time was made available by the University of California, Berkeley, Department of Mechanical Engineering. We gratefully acknowledge the continued technical support provided by the staff of the University of California, Berkeley, Mechanical Engineering workshops. Finally, thanks are due to Patricia Boughtin for the typing of this manuscript. The contents of this manuscript were presented as a paper at the ASME Winter Annual Meeting in Chicago, November, 1980.

REFERENCES

1. A. Abhat, Latent heat thermal energy storage in the temperature range 20–80°C, First Seminar on Solar Energy Storage; Thermal Storage, Trieste–Miramare, Italy (Sept. 1978).
2. Anon, Qualitative behavior of a new latent heat storage device for solar heating/cooling systems, General Electric Corporate Research and Development, Power Systems Laboratory (March 1977).
3. J. Stefan, Über die Theorie der Eisbildung insbesondere über die Eisbildung in Polarmaere, *Ann. Phys. Chem.*, **42**, 269 (1891).
4. J. D. Muehlbauer and J. E. Sunderland, Heat conduction with freezing or melting, *Appl. Mech. Rev.* **18**(12), 951–958 (1965).
5. H. G. Landau, Heat conduction in a melting solid, *Q. Appl. Math.* **8**(1) 81 (1950).
6. W. D. Murray and F. Landis, Numerical and machine solutions of transient heat conduction problems involving phase change, *J. Heat Transfer* **81C**, 106 (1959).
7. H. S. Carslaw and J. C. Jaeger *Conduction of Heat in Solids*, 2nd ed. Oxford University Press, Oxford 1978.
8. E. M. Sparrow, S. V. Patankar and S. Ramdhyani, Analysis of melting in the presence of natural convection in the melt region, *J. Heat Transfer* **99C**, 520–526 (1977).
9. N. W. Hale, Jr. and R. Viskanta, Photographic observation of the solid/liquid interface motion during melting of a solid heated from an isothermal wall, *Lett. Heat Mass Transfer* **5**, 329–337 (1978).
10. A. G. Bathelt, R. Viskanta and W. Leidenfrost, Experiments on the role of natural convection and heat source arrangement in the melting of a solid, *ASME paper* 78-HT-47 (Feb. 1978).
11. E. M. Sparrow, R. R. Schmidt and J. W. Ramsey, Experiments on the role of natural convection in the melting of solids, *J. Heat Transfer* **11**, 11–16 (1978).
12. A. G. Bathelt, R. Viskanta and W. Leidenfrost, An experimental investigation of natural convection in the melted region around a heated horizontal cylinder, *J. Fluid Mech.* **90**(2), 227–239 (1979).
13. R. N. Smith, T. E. Ebersole and F. P. Griffin, Heat exchanger performance in latent-heat thermal energy storage, *ASME paper* 79-HT-17 (1979).
14. M. Telkes, Storage of solar heating/cooling, ASHRAE Annual Meeting (June 1974).
15. W. R. Humphries, Performance of finned thermal capacitors, NASA T.N.D.-7690 (July 1974).
16. W. R. Humphries and E. I. Griggs, A design handbook for phase change thermal control and energy storage devices, NASA T. P. 1074 (Nov. 1977).
17. W. M. Rosenhow and H. Y. Choi, *Heat, Mass and Momentum Transfer*, p. 108. Prentice-Hall, Reading, MA (1961).
18. M. Telkes, Solar heat storage, ASME paper 64-WA/SOL-9 (1964).
19. S. Globe and D. Dropkin, Natural convection heat transfer in liquids confined to two horizontal plates and heated from below, *J. Heat Transfer* **81C**, 24 (1959).
20. D. V. Boger and J. W. Westwater, Effect of buoyancy on the melting and freezing process, *J. Heat Transfer*, **89**(1), 81–89 (1967).
21. I. Catton and D. K. Edwards, Effect of side walls on natural convection between horizontal plates heated from below, *J. Heat Transfer* **89**(4), 295–299 (1967).
22. B. Carnahan, H. A. Luther and J. O. Wilkes, *Applied Numerical Methods*, pp. 441–446. John Wiley, New York (1969).
23. Materials Engineering, 1979, *Materials Selector*. Reinhold, New York (Decemb. 1978).
24. R. Henze, Enhanced heat conduction in phase-change thermal energy storage devices, M.Sc. Thesis, University of California, Berkeley (1980).
25. J. A. C. Humphrey, Effect of turbulence on the precision of velocity and velocity fluctuation data obtained by photochromic visualization, *Can. J. Chem. Engng* **55**, 126 (1977).

ACCROISSEMENT DE LA CONDUCTION THERMIQUE DANS DES DISPOSITIFS DE STOCKAGE D'ENERGIE PAR CHANGEMENT DE PHASE

Résumé—Des dispositifs de stockage d'énergie par changement de phase ont un désavantage inhérent aux propriétés d'isolation présentées par les matériaux à changement de phase (MCP). De tels systèmes sont difficiles à analyser théoriquement à cause des non-linéarités de l'interface mobile liquide–solide et de la présence de convection naturelle, comme le montrent quelques études numériques et expérimentales récentes. Un travail antérieur a été insatisfaisant dans la prévision de performance de dispositifs en présence d'ailettes et de convection naturelle. Cette étude présente un modèle numérique simplifié, basé sur une équation quasi-linéaire de régime variable et pour ailette mince, qui prédit la fraction de MCP fondu et la forme de l'interface liquide–solide en fonction du temps avec une précision suffisante pour des objectifs pratiques. Des résultats expérimentaux sont comparés sous forme adimensionnelle avec des résultats du modèle et on constate un très bon accord. Pour obtenir des flux élevés de chaleur avec une quantité donnée de MCP et de métal, le modèle montre que la fusion du MCP dans un mode de conduction pure avec des ailettes fines et serrées est préférable à celle avec des ailettes plus épaisses et plus écartées, même avec intervention de la convection naturelle.

VERBESSERTE WÄRMELEITUNG IN LATENTWÄRMESPEICHERN

Zusammenfassung — Latentwärmespeicher haben von Natur aus den Nachteil der isolierenden Wirkung des Speichermaterials. Solche Systeme sind wegen der Nichtlinearitäten der beweglichen Fest-Flüssig-Grenzfläche und wegen des Auftretens freier Konvektion theoretisch schwer zu berechnen — wie in letzter Zeit mehrere numerische und experimentelle Untersuchungen gezeigt haben. Bisher ist es nicht gelungen, das Verhalten von Latentwärmespeichern mit Rippen bei freier Konvektion zu berechnen. Diese Studie beschreibt ein vereinfachtes numerisches Modell auf der Grundlage einer quasilinearen instationären Gleichung für dünne Rippen, mit deren Hilfe sich der Anteil des geschmolzenen Speichermaterials und die Form der Grenzfläche an der Schmelzfront als Funktion der Zeit mit für technische Zwecke ausreichender Genauigkeit berechnen läßt. Meßergebnisse werden in dimensionsloser Form mit Modellrechnungen verglichen und zeigen gute Übereinstimmung. Um bei einem gegebenen Aufwand an Speicher- und Rippenmaterial möglichst viel Wärme übertragen zu können, ist es nach diesem Modell günstiger, das Speichermaterial durch reine Wärmeleitung bei eng geteilten Rippen zu schmelzen, als dickere und weiter geteilte Rippen zu verwenden, selbst wenn dabei freie Konvektion auftritt.

ИНТЕНСИФИКАЦИЯ ТЕПЛОПРОВОДНОСТИ В АККУМУЛЯТОРАХ ТЕПЛОВОЙ ЭНЕРГИИ, ОСНОВАННЫХ НА ФАЗОВОМ ПЕРЕХОДЕ

Аннотация — Характерным недостатком аккумуляторов энергии, основанных на изменении агрегатного состояния вещества, является то, что используемые рабочие среды обладают теплоизолирующими свойствами. Такие системы трудно исследовать теоретически из-за нелинейностей, обусловленных перемещением границы раздела жидкость-твердое тело и естественной конвекцией, как это было показано в ряде последних работ. Предпринятая ранее авторами попытка исследовать работу таких аппаратов при наличии оребрения и естественной конвекции оказалась безуспешной. В данной работе приведена упрощенная численная модель, основанная на квазилинейном нестационарном уравнении для ребра небольшой толщины, которая позволяет с достаточной для практических целей точностью рассчитать изменение во времени количества расплавленного вещества и формы поверхности раздела жидкость-твердое тело. Получено хорошее согласие экспериментальных данных с результатами модельных расчетов. Модель показывает, что при фиксированном объеме рабочей среды и наличии металлического оребрения ребра небольшой толщины и с небольшим шагом обеспечивают более высокую интенсивность теплового потока при плавлении материала в режиме теплопроводности, чем ребра большей толщины и с большим шагом даже при наличии естественной конвекции.